Magnetotail Structure and its Internal Particle Dynamics During Northward IMF

M. Ashour-Abdalla, J. Raeder, M. El-Alaoui, V. Peroomian

Institute of Geophysics and Planetary Physics, University of California, Los Angeles, CA 90095-1567

This study uses Global magnetohydrodynamic (MHD) simulations driven by solar wind data along with Geotail observations of the magnetotail to investigate the magnetotail's response to changes in the interplanetary magnetic field (IMF); observed events used in the study occurred on March 29, 1993 and February 9, 1995. For events from February 9, 1995, we also use the time-dependent MHD magnetic and electric fields and the large-scale kinetic (LSK) technique to examine changes in the Geotail ion velocity distributions. Our MHD simulation shows that on March 29, 1993, during a long period of steady northward IMF, the tail was strongly squeezed and twisted around the Sun-Earth axis in response to variations in the IMF B_y component. The mixed (magnetotail and magnetosheath) plasma observed by Geotail results from the spacecraft's close proximity to the magnetopause and its frequent crossings of this boundary. In our second example (February 9, 1995) the IMF was also steady and northward, and in addition had a significant B_y component. Again the magnetotail was twisted, but not as strongly as on March 29, 1993. The Geotail spacecraft, located ~30 R_E downtail, observed highly structured ion distribution functions. Using the time-dependent LSK technique, we investigate the ion sources and acceleration mechanisms affecting the Geotail distribution functions during this interval. At 1325 UT most ions are found to enter the magnetosphere on the dusk side earthward of Geotail with a secondary source on the dawn side in the low latitude boundary layer (LLBL). A small percentage come from the ionosphere. By 1347 UT the majority of the ions come from the dawn side LLBL. The distribution functions measured during the later time interval are much warmer, mainly because particles reaching the spacecraft from the dawnside are affected by nonadiabatic scattering and acceleration in the neutral sheet.

1. INTRODUCTION

Over the past two decades, researchers have developed a number of global magnetohydrodynamic (MHD) models of the interaction of the solar wind with Earth's magnetosphere. These models have used as input various idealized solar wind conditions (e.g., where the IMF B_z is constant and northward or southward) to study the principal features of its coupling with the magnetosphere [*Leboeuf et al.*, 1978, 1981; *Lyon et al.*, 1981; *Brecht et al.*, 1982; *Ogino et al.*, 1984, 1985]. The actual state of the magnetosphere is far from being a simple superposition of idealized states [*Frank et al.*, 1995; *Raeder et al.*, 1995, 1997b] because

New Perspectives on the Earth's Magnetotail
Geophysical Monograph 105

the magnetosphere's internal evolution prevents it from responding in a simple, linear way to changes in the solar wind. Instead it is influenced by the history of the solar wind. While the solar wind varies on a time scale of minutes, the magnetosphere's internal evolution can take many hours to relax to a steady state. Consequently, in order to produce realistic configurations, it is necessary to use actual data from spacecraft located upstream in the solar wind as driving input to our models. Indeed recent MHD simulations with real data input can reproduce many of the changes in the global configuration of the magnetosphere [*Frank et al.*, 1995; *Raeder et al.*, 1997a, b; *Berchem et al.*, 1997a, b].

One of the goals of magnetospheric physics has been to understand the transport of plasmas through the solar wind-magnetosphere-ionosphere system. To attain such an understanding, it is necessary to determine the sources of plasmas, their trajectories through the magnetospheric electric and magnetic fields to the points of observation and the acceleration processes they undergo en route. There are too few spacecraft in the magnetosphere at any given time to make using observations alone an effective method of studying transport through the entire system. However, theory and modeling can be used to augment the available observations.

In this paper we detail an approach in which theory and numerical simulations are used in concert with observations to study plasma transport through the magnetospheric system. This approach is based on a global magnetohydrodynamic (MHD) simulation of the interaction between the solar wind and the magnetosphere which employs observed solar wind and interplanetary magnetic field (IMF) parameters to determine the solar wind boundary conditions and models the time-dependent response of the magnetosphere to the changing solar wind. We carefully calibrate the MHD model by comparing the fields and plasma moments from the model with observations within the magnetosphere, and when we are convinced a model is sound we use it to delineate plasma transport.

The MHD models yield a picture of the overall configuration of the magnetosphere and bulk transport, but the MHD paradigm neglects important physics such as particle drift motion. Magnetospheric observations show that plasma distribution functions are not simple thermal distributions. Instead they are frequently highly structured and complex [*Frank et al.*, 1995; *Ashour-Abdalla et al.*, 1996], and encoded in this complex structure is information about the transport and acceleration of the plasmas. We have developed a version of the large-scale kinetic (LSK) code [*Ashour-Abdalla et al.*, 1993] to extend the capability of MHD models by determining the history of the particles in the measured distribution functions. Starting from an observed distribution function we follow the trajectories of thousands of ions backwards in time through the electric and magnetic fields as determined from the corresponding MHD calculation [*El-Alaoui et al.*, 1995; *Ashour-Abdalla et al.*, 1997].

We apply this approach first to study the "quiet" magnetosphere when the IMF is northward for an extended period of time. Although the magnetosphere is less dynamic during intervals of northward IMF the magnetic configuration is still very complex. Observational, theoretical and simulation studies all indicate that when the IMF is northward for an extended period of time the magnetotail configuration is very different from the general configuration [*Frank et al.*, 1995; *Fairfield et al.*, 1996; *Raeder et al.*, 1995, 1997a, b; *Berchem et al.*, 1997a, b]. The simulation results support the observationally based evidence that high latitude reconnection between northward IMF field lines and tail field lines poleward of the polar cusps strongly influences the magnetospheric configuration [*Song and Russell*, 1992 and references therein]. For extremely prolonged periods of northward IMF, both observations [*Fairfield*, 1993] and simulations [*Ogino et al.*, 1992, 1994; *Usadi et al.*, 1993; *Raeder et al.*, 1995, 1997a; *Fedder and Lyon*, 1995] indicate that the magnetospheric configuration either is closed or has significantly reduced open field lines, resulting in the tail lobe having a smaller than average cross section. When the IMF has a B_y component the magnetotail can become twisted [*Cowley* 1981; *Brecht et al.*, 1981; *Ogino et al.*, 1985; *Frank et al.*, 1995; *Berchem et al.*, 1997a, b]. Field lines connecting the northern ionosphere twist to the southern hemisphere in the tail, and field lines from the southern ionosphere twist to the northern ionosphere, thereby giving the tail field lines a braided appearance [*Berchem et al.*, 1997a, b]. A changing B_y can cause the tail boundary to shift, resulting in a spacecraft near the magnetopause alternating between being in the magnetosheath and being in the magnetosphere [*Frank et al.*, 1995].

We briefly introduce the MHD model used throughout this study in section 2. Our first case study considers an interval from Geotail observations first noted by *Fairfield et al.* [1996]. On March 29, 1993, while the IMF remained steadily northward with constant sunward B_x, the B_y component changed from duskward to dawnward. We use this event to calibrate our MHD models by studying the response of the magnetosphere to the B_y component of the IMF during prolonged intervals of northward IMF. Our analysis of the configuration of the magnetosphere for this case is presented in section 3.

In the second case study presented in this paper, we address the question of ion transport through the magnetosphere during a period on February 9, 1995, when the IMF was northward and had a B_y component. In this study our goal is twofold: first we wish to ascertain the source of the

ions observed by Geotail in the near-Earth tail, and second, we wish to determine how these ions were accelerated after entering the magnetosphere.

Three main sources of magnetospheric particles have been identified: the low latitude boundary layer (LLBL), the plasma mantle and the ionosphere. Observations in the magnetotail near the equator identify the LLBL as a transition region through which plasmas can enter or leave the magnetosphere [*Hones et al.*, 1972a; *Eastman et al.*, 1976]. At higher latitudes in the tail, solar wind particles can enter the magnetosphere through the plasma mantle on open magnetospheric field lines [*Hones et al.*, 1972b; *Akasofu et al.*, 1973; *Rosenbauer et al.*, 1975; *Hardy et al.*, 1975; *Haerendel et al.*, 1978; *Pilipp and Morfill*, 1978]. The ionosphere, too, contributes plasma to the magnetosphere [*Shelley et al.*, 1972; *Geiss et al.*, 1978; *Lennartsson et al.*, 1979, 1981; *Lundin et al.*, 1980; *Balsiger et al.*, 1980; *Peterson et al.*; 1981; *Sharp et al.*, 1982; *Lennartsson and Shelley*, 1986]. *Shelley et al.* [1982] argue that the solar wind is the dominant source of ions in the magnetosphere at quiet times and that the ionosphere is dominant during more active times. *Chappell et al.* [1987] argue the ionosphere supplies enough ions to make up the entire ion component of the magnetosphere, an assertion which *Lennartsson* [1992] challenges.

Once inside the magnetosphere ions move through the magnetospheric electric and magnetic fields to the points of observation. Of special interest is the motion of ions near current sheets and neutral lines, where their behavior is sometimes nonadiabatic [*Speiser*, 1965; *Lyons and Speiser*, 1982; *Martin*, 1986; *Büchner and Zelenyi*, 1986, 1989; *Chen and Palmadesso*, 1986]. *Ashour-Abdalla* [1993, 1994, 1995] use the LSK approach with empirical magnetic and electric field models and demonstrate that the distant plasma sheet could be populated by the plasma mantle source. *Peroomian and Ashour-Abdalla* [1995, 1996] show that nearer Earth all three sources – the LLBL, the plasma mantle and the ionosphere – contribute to the plasma population and that the relative contribution of each source to the local distribution depends on the local time and radial distance from the Earth. *Richard et al.* [1994] and *Walker et al.* [1995, 1996] study the entry of particles into the magnetosphere by launching a distribution of solar wind ions into the electric and magnetic fields from a global MHD model. Their results show that for purely northward IMF is LLBL was the dominant source for solar wind ions, while for purely southward IMF the plasma mantle dominates, though the LLBL also contributes ions.

In section 4 we use the LSK method to investigate the source of ions observed by Geotail in the near-Earth plasma sheet during an interval on February 9, 1995, with steady northward, sunward and duskward IMF. We show how the sources change with time, leading to a complex distribution function even in the near-Earth plasma sheet during quiet times, and how nonadiabatic motion can influence the observed distribution function. We summarize our findings in section 5.

2. THE MHD MODEL

For this study we use a global MHD code that includes an ionospheric model to provide for the closure of field-aligned currents. In order to accommodate the large simulation volume with a 400 R_E tail and long simulation times, the simulation code has been parallelized for running on MIMD (Multiple Instruction - Multiple Data) machines by using a domain decomposition technique. The model essentially solves the ideal MHD equations, modified to include an anomalous resistivity term, for the magnetosphere and a potential equation for the ionosphere. Numerical effects, such as diffusion, viscosity, and resistivity, are necessarily introduced by the numerical methods. These permit viscous interactions and also, to a limited extent, magnetic field reconnection. However, the numerical scheme is optimized to minimize numerical effects. In particular, numerical resistivity is so low that it is necessary to introduce an anomalous resistivity term in order to model substorms correctly [see *Raeder et al.*, 1996]. The ionospheric part of the model takes into account three sources of ionospheric conductance: solar EUV ionization is modeled using the empirical model of *Moen and Brekke* [1993], diffuse auroral precipitation is modeled by assuming full pitch angle scattering at the inner boundary of the MHD simulation (at 3.7 R_E), and accelerated electron precipitation associated with upward field-aligned currents is modeled in accordance with the approach of *Knight* [1972] and *Lyons et al.* [1979]. The empirical formulas of *Robinson et al.* [1987] are used to calculate the ionospheric conductances from the electron mean energies and the energy fluxes. A detailed description of the MHD model, including initial and boundary conditions, can be found in *Raeder et al.* [1996, 1997b].

3. CASE I: MARCH 29, 1993

3.1. *Solar Wind Observations*

On March 29, 1993, from about 1200 UT to 2200 UT, the IMP 8 spacecraft was near (35, –16, –9) R_E in GSE coordinates, upstream of the bow shock in the dawn sector. Figure 1 shows the IMP 8 solar wind plasma and field measurements during this time period (black diamonds). The total magnetic field held fairly steady during the entire interval, rising slowly from about 12 nT at 1000 UT to about 15 nT at 2200 UT, which is about twice as strong as is usual for the solar wind. At about 1200 UT, the field

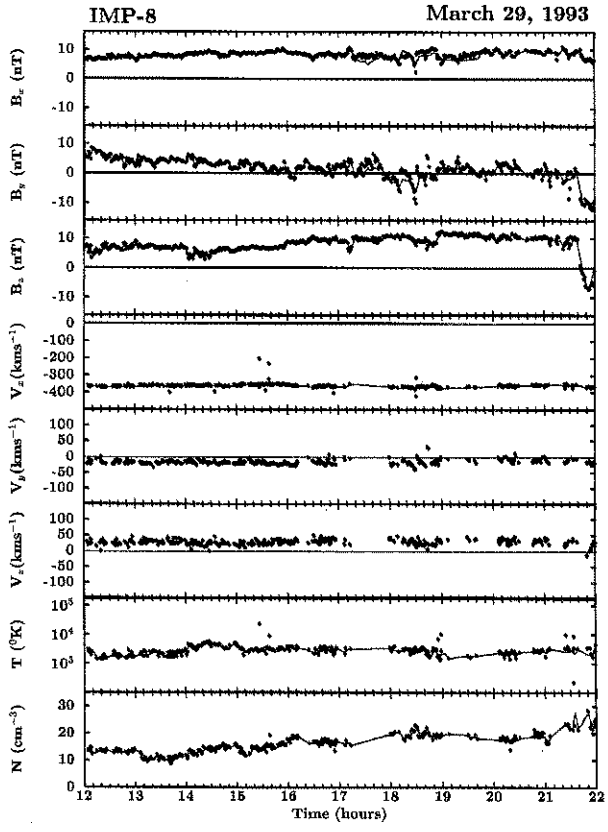

Figure 1. Solar wind parameters for March 23, 1993. The figure shows, from top to bottom: magnetic field components, velocity components, proton temperature, and proton density. The black dots indicate the IMP-8 measurements, and the red line shows the cleaned and averaged data that were used as input for the MHD simulation.

turned strongly northward and retained this northward orientation until 2130 UT. The IMF B_y component was fairly strong and positive at the beginning of the time interval, and until the end of the time interval it drifted slowly, almost linearly, towards zero. However, while B_z held fairly steady for most of the time interval of interest, B_y exhibited large fluctuations and sometimes changed sign. The IMF B_x component was quite large and steady with a value of about 8 nT throughout the time interval. The solar wind plasma measurements are less complete than the magnetic field measurements; however, inspection of Figure 1 shows that the solar wind density, velocity, and temperature were very steady, which allows us to interpolate and to fill in the missing values. The data also include some unrealistic and seemingly erroneous values in the plasma time series which we removed. Although the V_y and V_z solar wind velocity components were available, we did not use these data, but instead set V_y and V_z to zero, because the data not only had the same gaps that the other plasma parameters had but also fluctuated strongly on a short time scale (1 min), with amplitudes reaching a few degrees in direction. Because a one-degree deflection of the solar wind direction causes a 2.35 R_E deflection of the tail at the Geotail position (134 R_E downtail) we deemed these measurements not accurate enough for use in this study.

The red curves in Figure 1 show the processed solar wind data used as input to the model. Data gaps, primarily in the plasma data, were filled by interpolation or extrapolation. The input data are 3 minute averages and are produced by the solar wind model described in *Raeder et al.* [1996, 1997b]. The IMF **B** vector that is used as input is nearly identical to the observed IMF. However, around 1800 UT some strong rotations of the IMF vector occur that are not completely resolved by the solar wind model, and slight deviations of the input field from the measured field become visible. Although this is not entirely satisfactory, this solar wind model is the best that can be constructed with single point IMF measurements, because the alternative is to keep B_x constant and thereby miss some major rotations of the IMF vector.

3.2. Geotail Observations and Comparison with the MHD Model

During the latter half of March 29, 1993, the Geotail spacecraft was located in the distant tail, where it moved from its position at (–134.4, 14.4, –0.8) R_E (in GSE coordinates) at 1200 UT to (–132.4, 13.2, –0.9) R_E at 2200 UT. For a 370 km/s solar wind the aberration resulting from Earth's motion would cause the tail to rotate by 4.5° toward dusk, thus reducing the effective Geotail y position by 10.5 R_E. This rotation would put Geotail very close to the tail center, i.e., in aberrated coordinates the Geotail position would be near (–133, 3.5, –0.8) R_E. Additional tail aberrations, caused by a non-radial solar wind flow vector, may also be found in the data. *Fairfield et al.* [1996] estimate from the IMP 8 observations that the solar wind flow vector points on average 2.5° toward dawn and 2.6° towards north. Using this estimate, the Geotail position in aberrated coordinates would be near (–133, 9.3, –6.8) R_E, still relatively very close (11.5 R_E) to the tail center. We note, however, that the IMP 8 solar wind directional measurements fluctuate substantially during this time interval. By all estimates, Geotail was very close to the tail center at this time, and it is thus expected that it observed only plasmas and fields that are typical for the tail.

Figure 2 shows the Geotail plasma and magnetic field observations at 48 s time resolution from 1200 UT to 2200 UT on March 29, 1993 (black curves), results from the

MHD model with no aberration (red curves), with nominal (only Earth motion) aberration (green curves), and with the aberration vector estimated by *Fairfield et al.* [1996] (blue curves).

The Geotail observations can be ordered most easily by the x component of the velocity (V_x). During most of the interval V_x is between –400 km/s and –350 km/s, which is close to the observed solar wind velocity. At these times, the ion density is fairly high, near 10 cm^{-3}, and the plasma is cool, about 2×10^5 °K. Apparently, Geotail is in the magnetosheath during these times or possibly in a boundary layer with plasmas and fields that are very like the magnetosheath. Between these time intervals of magnetosheath-like plasmas and fields, the tailward velocity drops notably, the plasma is at least one order of magnitude hotter, the density is at least one order of magnitude lower, and the magnetic field assumes a tail-like orientation. Before 1900 UT this tail-like orientation corresponds to the southern lobe. Later, the direction is that expected for the northern lobe.

The colored curves show the MHD results for three aberration angles that lie within a cone of about 5°. None matches the observations very well. However, taken together, they essentially bracket B_x and V_x. B_x and V_x have sharp spatial gradients and therefore are the most revealing quantities of the tail topology. It is reasonable to assume that the tail boundary corresponding to these gradients is also well bracketed by the simulation results. As we show later, this boundary is the distant tail magnetopause. Small changes in the aberration angle, which are about of the same order as the accuracy of the solar wind directional measurements, cause drastic changes in the model output. Thus, even if we had a perfect model, it would be necessary to know the solar wind direction to within a few tenths of a degree in order to predict the Geotail observations accurately. Given the limitations of the solar wind measurements and the inaccuracies that are inherent in our model, in particular the coarse resolution in the distant tail (about 1.5 R_E in y and z, and about 5 R_E in x), the comparison is reasonably good. This assessment also holds for the B_y and B_z magnetic field components, except for small scale fluctuations that are beyond the realm of the model. In particular, the model predicts, in accordance with the observations, a B_y component that slowly drifts from positive to negative values, and a strongly positive B_z. The V_y and V_z components are also basically in accordance with the observations, considering that they are also affected by the solar wind aberration. In particular, the model predicts slightly duskward flows, i.e., the flow vector is oriented towards the tail center. Because of the low resolution, the model fails to predict the sharp gradients in the plasma density and temperature, i.e., these quantities are somewhat smeared out over the grid and the predictions generally fall between the extremes of the observed values.

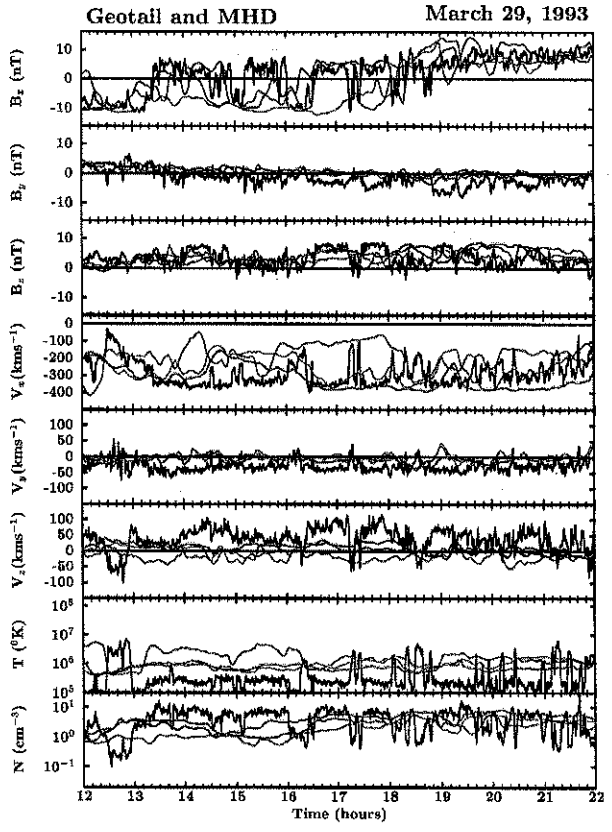

Figure 2. A comparison of time series from Geotail (black curves) and the MHD simulation (colored curves based on different assumptions of aberration; see text). The figure shows, from top to bottom: magnetic field components, velocity components, proton temperature, and proton density.

3.3. The Tail Cross Section at Geotail

Figures 3a and 3b show y_{GSE} - z_{GSE} cross sections at the Geotail position, i.e., at x = –134 R_E, at different times. The left panels show the color coded magnetic field's B_x component, and lines that are tangential to the magnetic field projection in the y_{GSE} - z_{GSE} plane. The right panels show the color coded V_x component of the flow and the (V_y, V_z) vectors. The dots indicate the Geotail position, according to the different tail aberration assumptions. The color of the dots corresponds to the colors in Figure 2: red is the nonaberrated position, green the position with nominal (only Earth motion) aberration, and blue the *Fairfield et al.* [1996] estimate. The six snapshots correspond to 1200 UT, 1400 UT, 1500 UT, 1700 UT, 1900 UT, and 2100 UT, respectively.

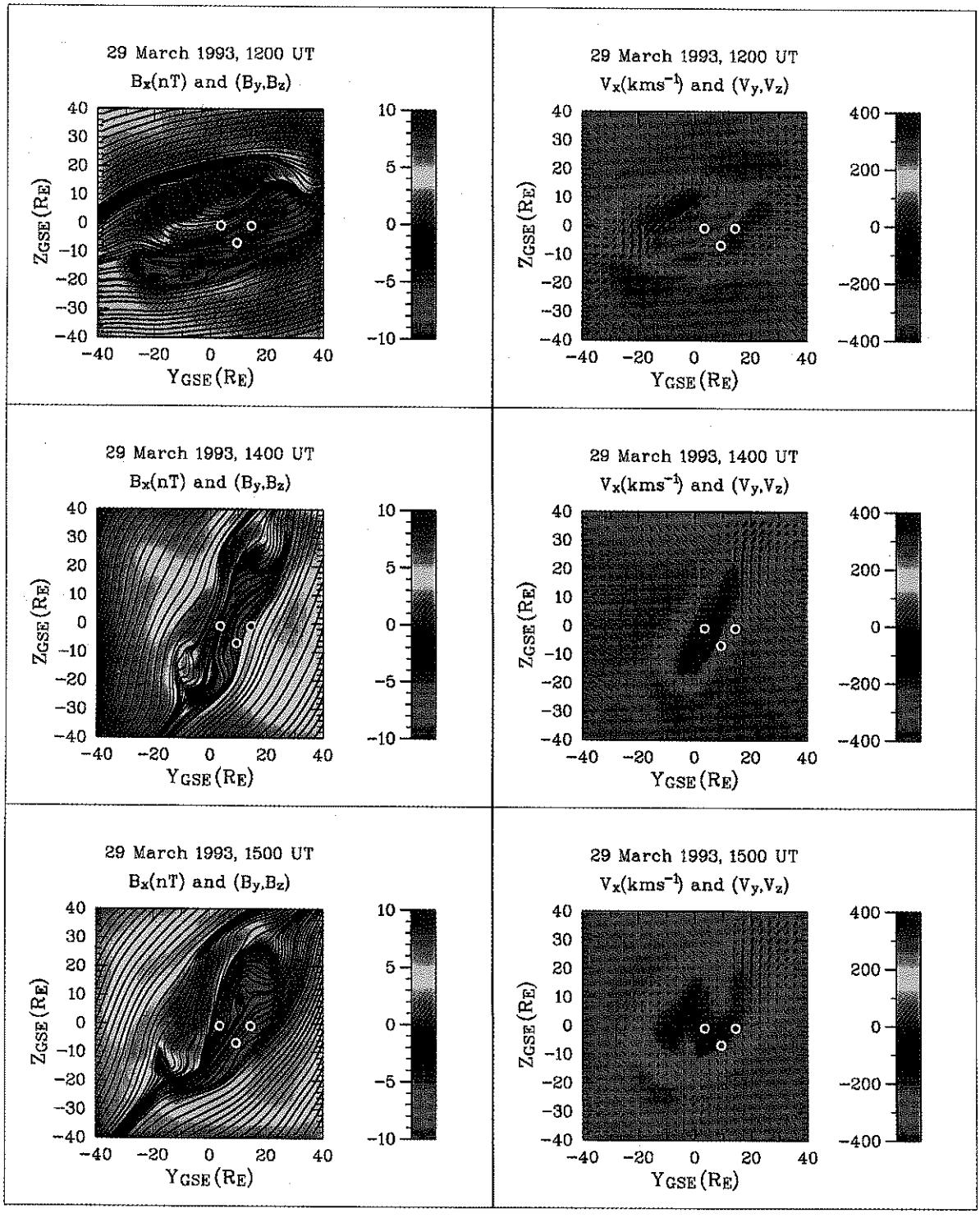

Figure 3. (a) Cross sections of the tail at the Geotail location ($x_{GSE} = -134\ R_E$) at 1200 UT, 1400 UT, and 1500 UT. The left panels show the color-coded magnetic field B_x component and lines that are tangential to the field. The right panels show the color coded V_x velocity component along with the (V_y, V_z) velocity vectors. The colored dots indicate the Geotail location in the y_{GSE}-z_{GSE} plane according to different assumptions of aberration (see text for details); (b) Similar to (a), but at 1700 UT, 1900 UT, and 2100 UT.

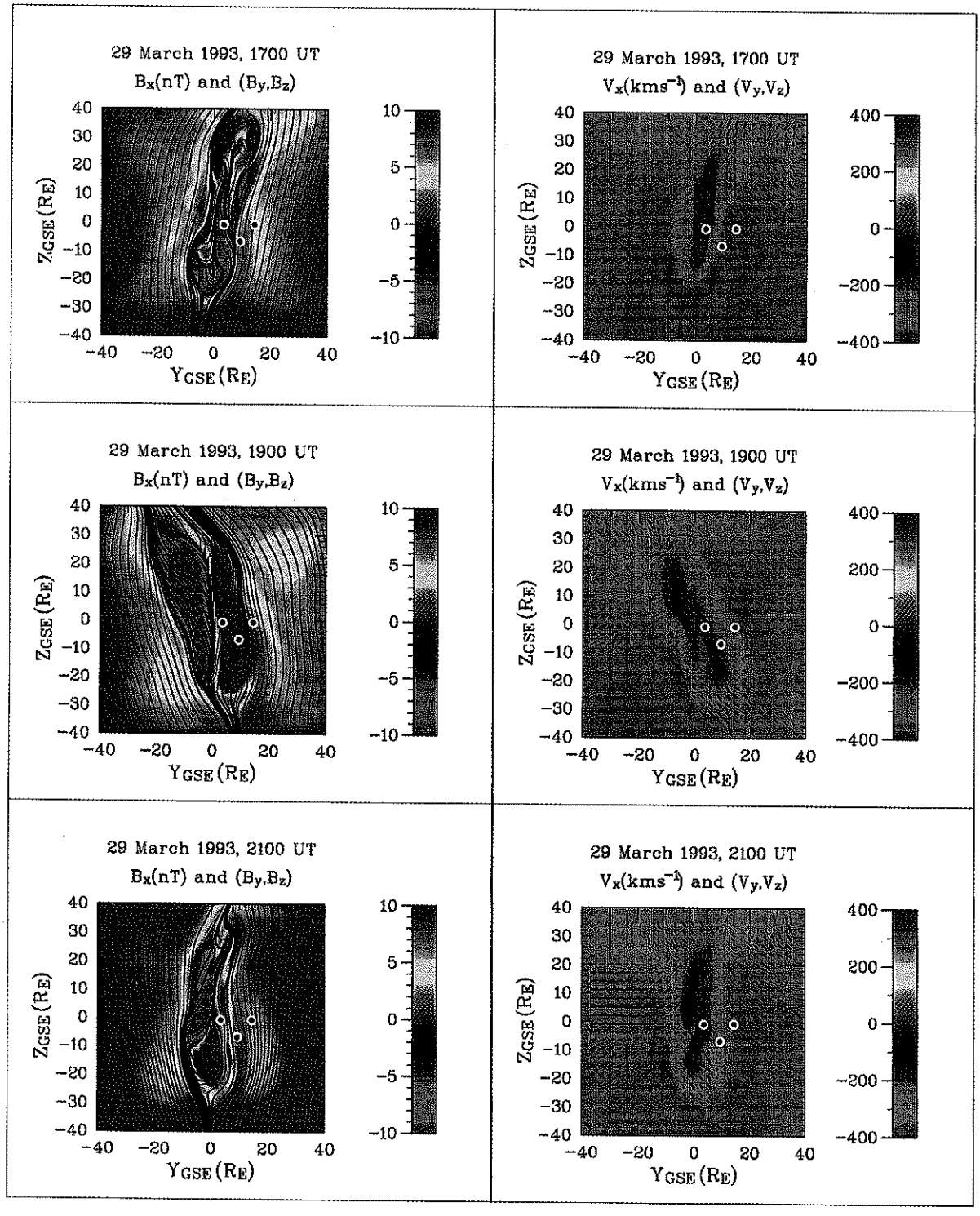

Figure 3. Continued from previous page.

At 1200 UT, Geotail is located in the southern lobe (compare with Figure 2). The lobe at this time is not circular, as many models predict (see, for example, *Sibeck et al.*, 1986), but instead is flattened and twisted. The overall shape of the tail is roughly elliptical, with the semimajor axis about twice as large as the semiminor axis. The flow velocity is lowest in the lobes. In the magnetosheath and the tail plasma sheet, it is comparable to the solar wind velocity.

At 1400 UT, the lobe has become even more flattened and twisted. Along the minor axis, the tail dimension is reduced to about 20 R_E, while the major dimension is about 80 R_E. At the same time, the lobe is twisted by almost 90 degrees counter-clockwise as viewed from the sun, such that the northern lobe is in the dawn sector and the southern lobe is in the dusk sector. Except for the case of nominal aberration, the Geotail position is very close to the magnetopause. The Geotail observations (Figure 2) show that Geotail is at this time in a region of magnetosheath like plasma and fields.

At 1500 UT the tail has somewhat relaxed and now looks more like that at 1200 UT. This rotation and the increase of the minor dimension, given our assumptions regarding tail aberration, put Geotail back into the southern lobe at this time. Unlike the 1200 UT and 1400 UT intervals, the plasma sheet at 1500 UT is inclined by about 20 degrees with respect to the major axis.

At 1700 UT, the tail has narrowed again and is twisted to an almost upright orientation. As was the case around 1400 UT, the minor dimension is reduced to about 20 R_E, leaving Geotail in magnetosheath-like plasmas and fields. However, this case is different from that for 1400 UT, in that the northern lobe lies mainly in the northern hemisphere and the southern lobe lies mainly in the southern hemisphere. However, there are some structures of opposite sign in both hemispheres.

A dramatic change has occurred by 1900 UT. While at earlier times the tail was twisted such that the northern lobe tended to be on the dawn side and the southern lobe on the dusk side, the opposite is now true. The fact that the tail has also expanded somewhat results in Geotail's now being in the northern lobe for the first time. Inspection of Figure 2 reveals that after this time Geotail does not enter the southern lobe again for the subsequent 3 hours. However, the observations indicate that from this point on, Geotail repeatedly enters the northern lobe because B_x stays positive during intervals of low density and high temperature. The simulation shows exactly the same picture.

At 2100 UT, the tail has essentially retained its previous structure. However, the twisting angle has become considerably larger than 90 degrees. As a consequence, the northern lobe is at this point entirely in the southern hemisphere and vice versa.

A number of features are common to the tail cross sections at all times. First, the major axis of the elliptically distorted tail is always aligned with the magnetosheath field direction in the y - z plane. This behavior of the tail is similar to that found in ISEE-3 data by *Sibeck et al.* [1985, 1986], who deduced a tail cross section of similar shape, but with the major axis in the east-west direction. Second, the flow in the magnetosheath is primarily directed towards the tail center where the tail dimension is smallest and away from the tail center at the "long ends." This is consistent with a flaring of the tail in the larger dimension, and a negative flaring, i.e., convergence, in the smaller dimension. Third, the flow velocities in the lobes are not uniform. Towards the magnetopause, the velocities are about 100 - 200 km/s smaller than the magnetosheath velocity. Towards the tail center, the velocity becomes very small, of the order of 100 km/s or less. This indicates that the topology of the inner part of the tail is different from that of the outer part. Because of the strong northward IMF, the outer part may well be a boundary layer just inside the magnetopause. Such a broad boundary layer has been found in earlier studies of the middle tail [*Raeder et al.*, 1997*b*], but little is known about its extension into the distant tail. Fourth, the simulation results show that Geotail traverses the distant tail magnetopause when it observes steep gradients in the plasma and field parameters. Such an interpretation is not obvious from the Geotail observations alone, and *Fairfield et al.* [1996] suggest that the magnetosheath-like plasmas and fields may be a signature of a closed tail.

In summary, our global simulation for March 29, 1993, shows that the structure of the distant tail under strongly northward IMF conditions is quite different from that predicted by simple models. The simulation results are in basic accordance with the Geotail observations and provide a framework for interpreting the data. However, additional analysis will be required to determine why the tail reacts to northward IMF in this way. This issue will be the topic of a forthcoming study.

4. CASE II: FEBRUARY 9, 1995

4.1. Observations

On February 9, 1995, between 0800 UT and 1400 UT the Wind spacecraft was located at (190, 40, 2) R_E in Earth-centered solar-ecliptic (GSE) coordinates. The solar wind magnetic field observations in Figure 4 were provided by the GSFC magnetometer on Wind [*Lepping et al.*,

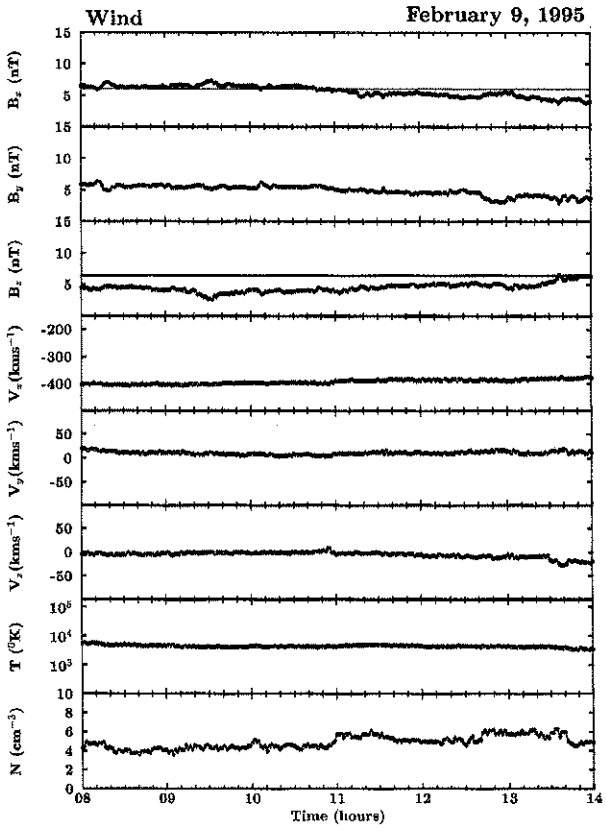

Figure 4. Solar wind parameters on February 9, 1993. The figure shows, from top to bottom: magnetic field components, velocity components, proton temperature, and proton density. The black dots indicate Wind measurements, and the red line shows the cleaned and averaged data that were used as input for the MHD simulation.

1995], while the plasma parameters were obtained from the Solar Wind Experiment (SWE) [*Ogilvie et al.*, 1995]. We use Wind data as input to the MHD model, even though the spacecraft was far from Earth, because it is the only solar wind monitor available. (Although IMP-8 was closer to Earth it was not in the solar wind at this time.) The IMF and the solar wind parameters were very stable for the entire 6 hours. During this time interval of steady northward IMF (B_z = 5 nT), there was also a significant positive B_y component (B_y = 5 nT) to the IMF which was comparable to its B_z component. The values of the solar wind speed, density, and thermal pressure were about 400 km/s, 5 cm^{-3}, and 3.5 pPa, respectively, consistent with the average solar wind.

During this time interval the Geotail satellite was located in the tail, and moved from (–31.0, 3.0, –3.0) R_E to (–27.8, –0.6, –2.3) R_E (GSE). Three-dimensional distribution functions were obtained from the Hot Plasma Analyzer (HP) of the Comprehensive Plasma Instrumentation (CPI) [*Frank et al.*, 1994]. For the observations presented here, the HP analyzer was operated in a mode in which the ion velocity distributions were determined, with more than 3000 samples falling within the energy-per-unit charge (E/Q) range of 22 V to 48 kV with a repetition rate of 22 s. Figure 5 shows V_y - V_z, V_x - V_z, and V_x - V_y cuts of the 3-D Geotail ion distribution functions in GSE coordinates. The two rows in this figure correspond to cuts of the Geotail velocity distribution functions for the 1325 UT and 1347 UT time intervals. The arrows show the direction of the magnetic field projected onto the x - z plane. At 1325 UT, the ion distribution exhibits counterstreaming structures in the direction parallel to **B** and relatively cold structures in the direction perpendicular to **B**. Geotail was in the southern plasma sheet boundary layer (PSBL) at this time since $B_x < 0$ and is the largest component (Figure 6). By 1347 UT, Geotail observed earthward flow and a stronger B_z, suggesting that the spacecraft was in the outer central plasma sheet (CPS). The perpendicular temperature of the ion distribution at 1347 UT was higher than in the earlier time period.

4.2. Comparison of Geotail Observations with the MHD Model

Our previous example (March 29, 1995) demonstrated that the magnetosphere displays a great deal of complexity that is a consequence of the interaction between external driving, i.e. the IMF and the solar wind, and the magnetosphere's internal evolution. This effect is also seen in our second example, February 9, 1995, when the magnetosphere was not in a steady state despite an IMF and a solar wind that were steady for more than 6 hours.

IMF and plasma data from the Wind spacecraft on February 9, 1995 (Figure 4), were used as input to the global MHD simulation outlined in section 2. The red curves in Figure 4 indicate the values used as input in the MHD simulation. Note that a constant B_x was used in the simulation. Late in the simulation run this caused us to overestimate the value of B_x.

Figure 6 shows as black curves the magnetic field (B_x, B_y, B_z), the three components of the velocity (V_x, V_y, V_z), the ion temperature (T), and the number density (N) observed by the Geotail magnetometer [*Kokubun et al.*, 1994] and CPI versus time from 1200 UT to 1400 UT. The magnetic field data are 3-second averages while the resolution of the plasma moments is 64 seconds. The time series from the MHD simulation at the location of Geotail are

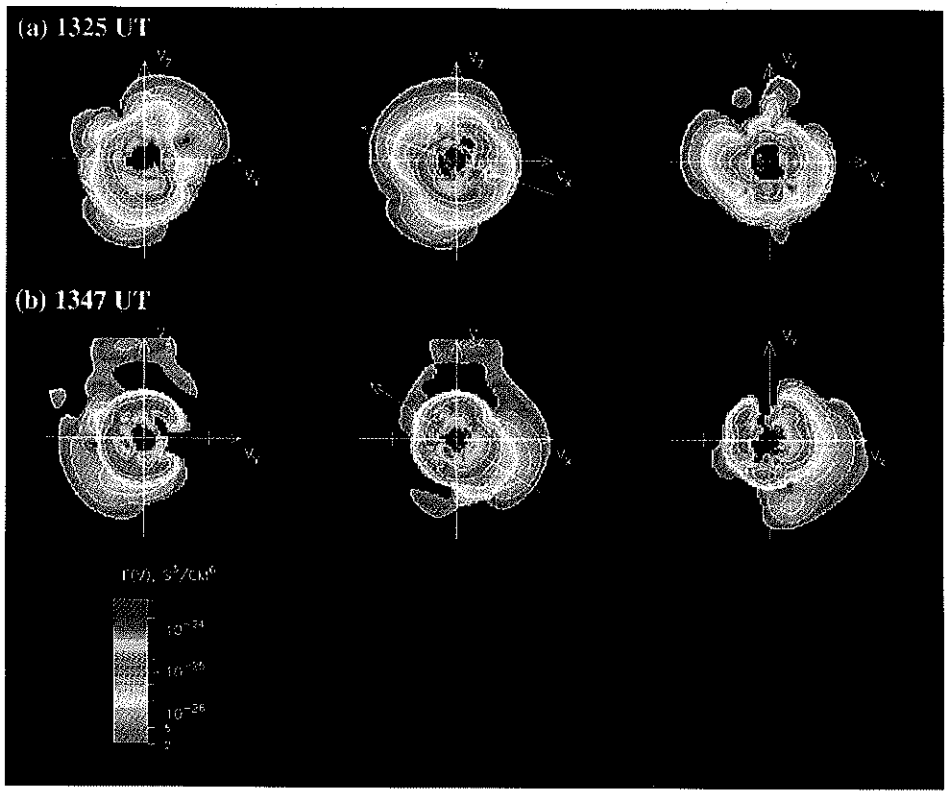

Figure 5. Cuts of the three-dimensional Geotail velocity distribution functions from the CPI instrument for 1325 UT (upper row) and 1347 UT (lower row). The three panels in each row correspond to V_y - V_z, V_x - V_z, and V_x - V_y cuts, and the arrows indicate the projection of the average magnetic field onto the plane of the cut.

plotted in green. The simulation does a poor job of reproducing the observations. The reason for this can be seen in Figure 7 where we have plotted B_x and V_x in the y - z plane and V_x in the x - z plane at 1325 UT and 1347 UT. The location of Geotail is shown by a blue dot. Throughout this interval in the simulation Geotail is in the southern tail lobes, just outside of the PSBL. This is a region of steep gradients in the field and plasma parameters. The MHD model cannot resolve phenomena on scales smaller than a few grid points. During this interval the grid spacing is $\Delta x = 0.95\ R_E$, $\Delta y = 0.50\ R_E$, and $\Delta z = 0.50\ R_E$. In addition to uncertainties caused by the grid spacing, errors in the location of the spacecraft with respect to magnetospheric boundaries can result from the use of constant IMF B_x in the simulations and because we didn't update Earth's dipole tilt during the simulation. A displacement of a few grid spaces would greatly change the location of Geotail with respect to the physical boundaries in the magnetotail.

As can be seen in Figure 6, the simulation does an especially poor job of reproducing the observations in the interval between 1200 UT and 1300 UT. In particular the simulation does not reproduce the observed strong Earthward flows ($V_x \approx 200$ km/s). The reason for this can be seen in Figure 7, which shows that in the simulation the flow diverges just earthward of the spacecraft position with earthward flows about 4 R_E or 5 R_E earthward of Geotail. Displacing Geotail 5 R_E in x, 2 R_E in y, and 1 R_E in z yields the blue curve in Figure 6. This displacement moves the spacecraft into the earthward flow region and more closely reproduces B_x as well. However, now the model gives strong earthward flows between 1300 UT and 1400 UT, flows that are not observed.

After trying many different displacements we concluded that it is not possible to find any single displacement which can correct the model for the entire interval. The variability of the results in Figure 6 strongly suggests that

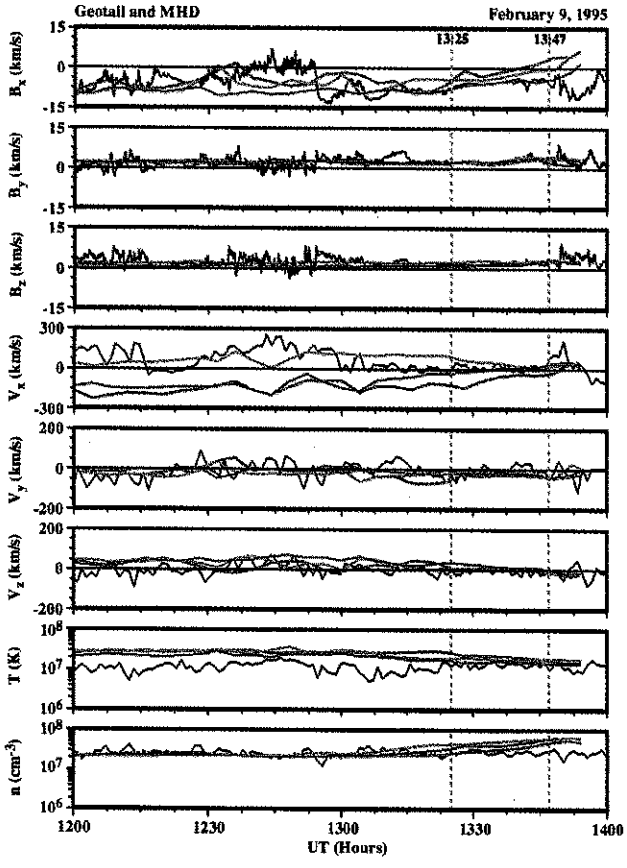

Figure 6. A comparison of time series from Geotail (black curves) and the MHD simulation (colored curves according to different spacecraft displacement, see text). The figure shows, from top to bottom: magnetic field components, velocity components, proton temperature, and proton density. The vertical yellow lines indicate the times at which particles from measured distribution functions where launched in the model.

the magnetosphere remains dynamic even when the IMF is northward for a long period of time. As the magnetosphere changes the gradients change, and this causes the error in the model to change. Therefore we decided to try to optimize the MHD model only for this study's interval of prime interest. Accordingly, we looked for displacements giving the best fit for the Geotail observations between 1300 UT and 1400 UT. During this interval the ions observed at 1325 UT and 1347 UT enter the magnetosphere and travel to Geotail. The red curve in Figure 6 gives the desired best fit to the observed values between 1300 UT and 1400 UT. It was obtained by displacing Geotail by 0 in x, 1.5 R_E in y, and 0.5 R_E in z. Except for giving too large a number density the fit is very good. Although this good fit to observations from one spacecraft is no guarantee that the MHD model is correct, it is the best indicator that we presently have.

The magnetospheric configuration at this time is very complex. Figure 8 shows a perspective view of the magnetosphere at 1312 UT. The three color contours shown in this figure correspond to the total current density from the MHD simulation in the $x = -30\ R_E$, $x = -90\ R_E$, and $x = -150\ R_E$ planes. The overall topology of the magnetosphere remains relatively unchanged during the simulation, and these planes are representative of the entire interval. Geotail's location, which is around $x = -28.2\ R_E$, $y = -0.2\ R_E$, and $z = -2.4\ R_E$, is indicated by the white dot. Characterized by large current densities, the current sheet and the magnetopause are clearly discernible. The structure of the plasma sheet has undergone significant changes as a result of the more than 5 hours of steady northward IMF with a significant B_y component. Because of the IMF B_y, the current sheet is twisted around the Sun-Earth axis toward the duskside at $x = -30\ R_E$, and this effect gets more pronounced further downtail. The field lines plotted in Figure 8 show that because of the twisting of the geomagnetic tail, portions of the northern (southern) lobe fall below (above) the equatorial plane, and field lines emanating from the northern (southern) hemisphere cross the equatorial plane and are found downtail in the opposite hemisphere, just as occurred on March 29, 1995 (previous section).

Figure 9 shows plots of field lines within 1 R_E of Geotail at the two times chosen for this study. At 1325 UT, the spacecraft is in a mixed region of open (red) and closed (blue) field lines. At 1347 UT, Geotail is mostly in a region of closed field lines. In order to gain a better understanding of the changes in the Geotail velocity distribution functions as the spacecraft traverses from a region of open to closed field lines, we integrate ion orbits backwards in time in a time-dependent large-scale kinetic (LSK) study, using the Geotail velocity distribution functions as input; the results are discussed below.

4.3. Sources of Ions for Geotail Distributions

As already noted, despite the quiet solar wind conditions observed on February 9, 1995, significant changes in the Geotail distributions occurred during this interval (Figure 5). In this section, we investigate the sources of the ions comprising the Geotail distributions in order to determine the origin and delineate the transport of magnetotail plasma during this seemingly quiet period.

Because of the time-dependent nature of the problem, we have used the time-dependent magnetic and electric fields

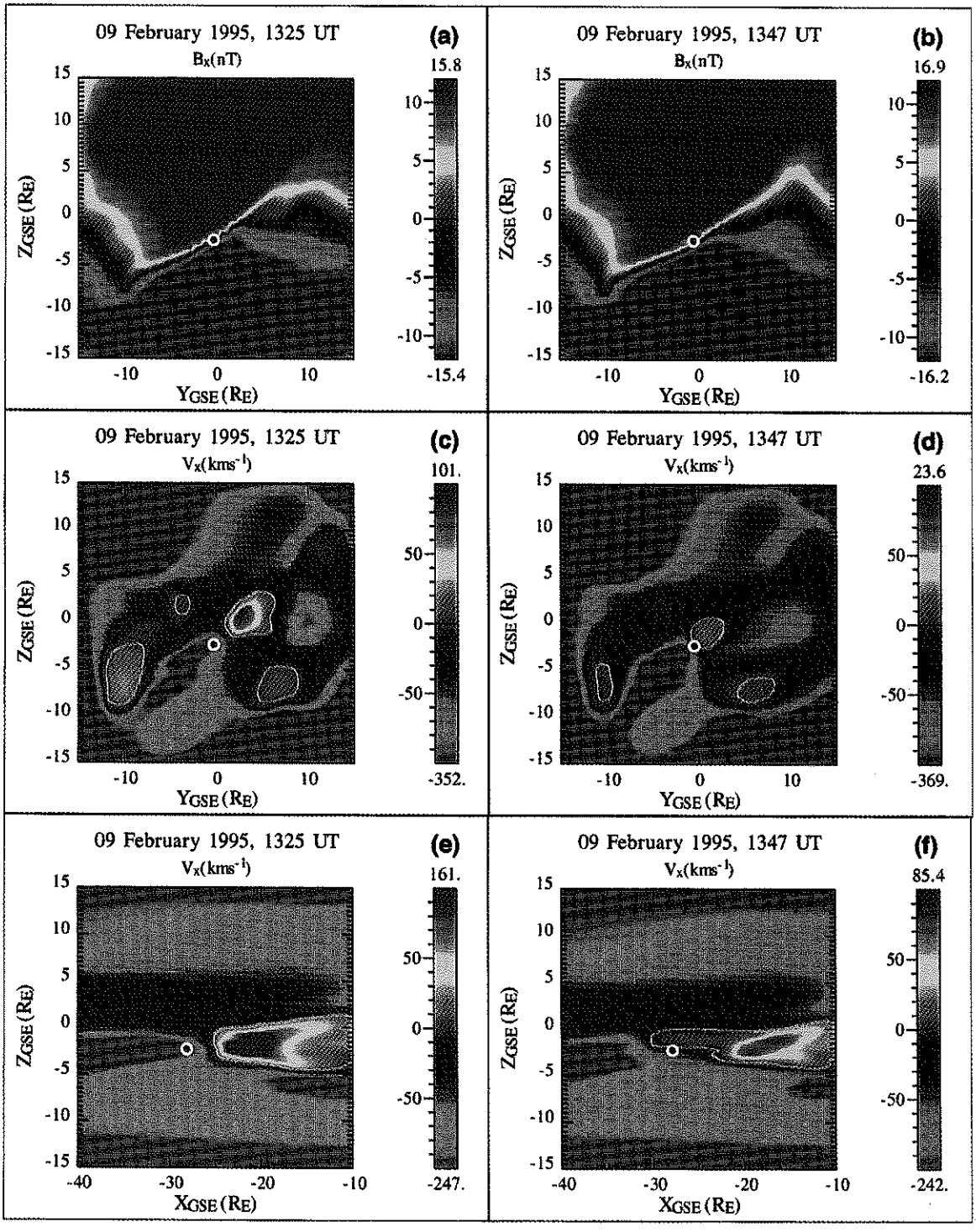

Figure 7. Top panel: Cross sections of the tail at the Geotail location ($x = -29\ R_E$) at 1325 UT and 1347 UT. The magnetic field component B_x is color coded. Middle panels: Same as top panel, but the V_x component of the velocity is color coded. Lower panel: Like the middle panel, but a cut of the x_{GSE} - z_{GSE} plane through the Geotail location. The dots indicate the nominal Geotail location.

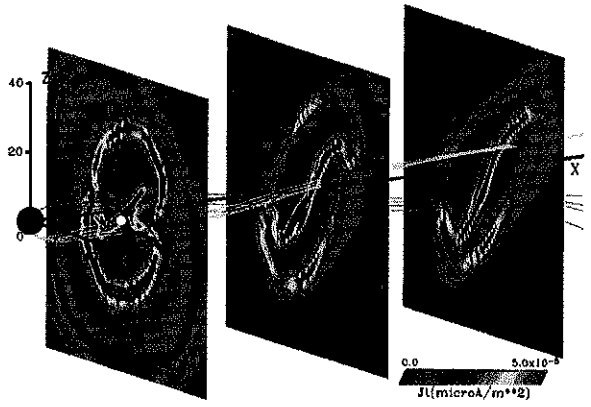

Figure 8. y - z cuts of the MHD current at 1312 UT on February 9, 1995, at $x = -30\ R_E$, $x = -90\ R_E$, and $x = -150\ R_E$. The white dot indicates the location of Geotail.

from the MHD simulation in our LSK calculation. The MHD electric field used in this calculation is given by:

$$\mathbf{E} = -\mathbf{v} \times \mathbf{B} + \eta \mathbf{J} \qquad (1)$$

where **v** is the bulk velocity, **B** is the local magnetic field, η is the resistivity which is a function of the local magnetic field gradients, and **J** is the local current density. The electric field has both a convective ($-\mathbf{v} \times \mathbf{B}$) and a resistive ($\eta \mathbf{J}$) term. The resistive term becomes important near the magnetopause and near x-lines but is negligible elsewhere. Starting with the Geotail distributions at 1325 UT and 1347 UT in Figure 5, we construct three-dimensional distributions in velocity space by placing ~90,000 ions in V_x - V_y - V_z bins (100 km/s × 100 km/s × 100 km/s) such that the number in each bin is proportional to the observed phase space density of that bin. One particle in the computational distribution function corresponds to 5×10^{-27} s^3cm^{-6} in the Geotail distribution function. Since the scale in Figure 5 ranges from 2×10^{-27} to 5×10^{-24}, the fine-scale structure of the observed distribution is preserved in the computational distribution function. For each particle we integrate the equation of motion ($d\mathbf{v}/dt = q\mathbf{v} \times \mathbf{B} + q\mathbf{E}$) backward in time until the particle encounters the magnetopause (defined by using the MHD currents) or the ionosphere (taken as the inner boundary of the MHD simulation, at $r = 3.7\ R_E$). Since the minimum grid spacing in the global MHD simulation is relatively large (~0.5 R_E), and the simulation data are saved at four minute time intervals, we use linear interpolation (over space and time) to determine the instantaneous values of the MHD fields on scales smaller than the grid spacing. We calculate the ion trajectories in the evolving magnetic and electric fields by using a fourth-order Runge-Kutta method. The time step in the particle trajectory calculation is nominally set to 0.002 times the local ion gyro-period, with an upper limit imposed to ensure that the time step does not get too large in weak field regions.

The two panels in Figure 10 show the entry points of the ions in the measured distribution functions shown in Figure 5. Each color-coded dot in the figure represents the number of ions originating from a $1\ R_E \times 1\ R_E \times 1\ R_E$ region centered at the point. The green sphere shows the location of Geotail, and the contour plot in each panel represents a cut of the MHD current in the $x = -150\ R_E$ plane at the time of the measurement and is shown to help locate the magnetopause.

Between 1325 UT and 1347 UT, Geotail slowly moves from the PSBL into the outer CPS. Figure 10*a* shows the entry points of particles seen by Geotail at 1325 UT, when the spacecraft has just entered the closed field line region. The total current in the y - z plane at x = -150 R_E is also

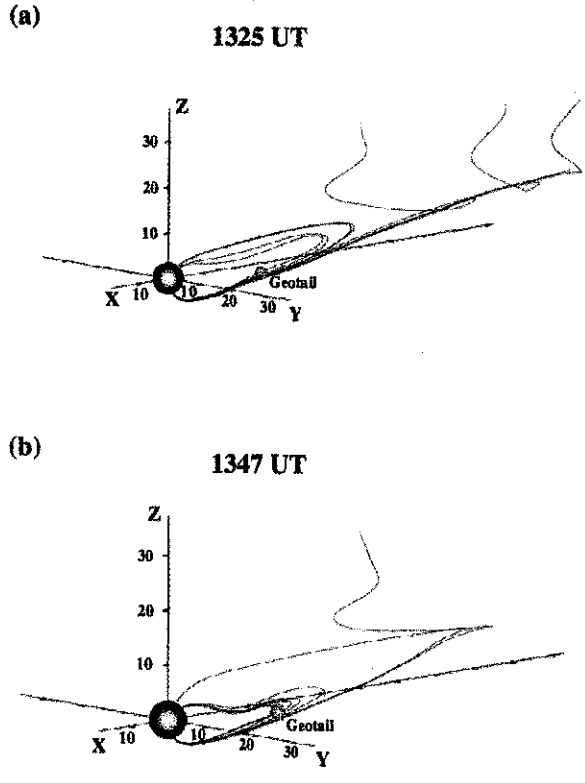

Figure 9. Plot of field lines for the two time intervals examined in the paper. Field lines within 1 R_E of the Geotail location are shown for each interval. Red field lines are open, and blue field lines are closed.

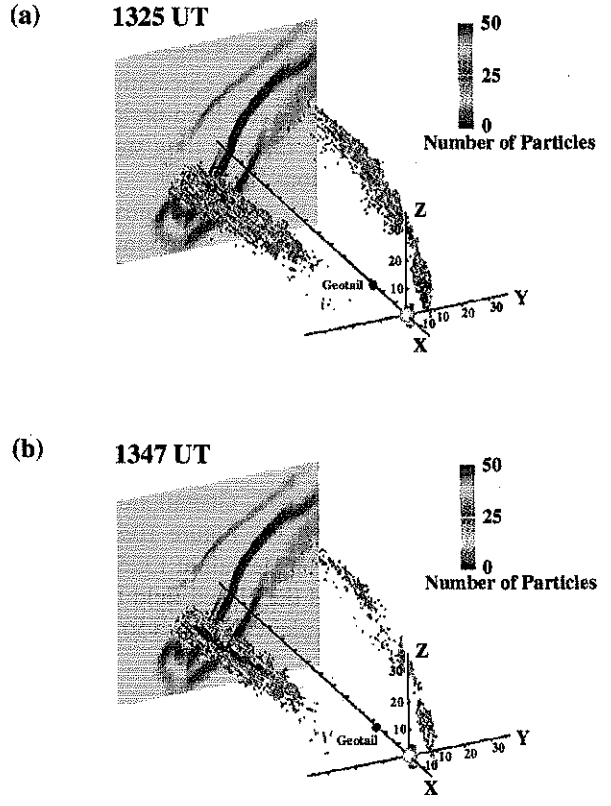

Figure 10. Magnetospheric entry plots for the two time intervals examined in the paper. The dots are color coded according to the number of particles originating from a 1 $R_E \times 1\ R_E \times 1\ R_E$ bin centered on the point. The total current in the $x = -150\ R_E$ plane is also shown in each panel.

plotted. This gives an indication of the relationship between the ion entry points and magnetospheric boundaries. Ions from both the dawn and the dusk side LLBL have access in nearly equal numbers to the Geotail location. Dawnside LLBL ions (50% of ions measured at Geotail) originate in a wide region in z centered at the equatorial plane extending between $-10\ R_E > x > -150\ R_E$. However, the bulk of the dawnside entry occurs tailward of $x = -100\ R_E$. As we shall see below, the dawnside ions are on primarily nonadiabatic orbits. These ions are responsible for the bulk plasma seen in the direction perpendicular to **B** in the Geotail velocity distribution functions at this time. The duskside LLBL is another major source of ions for this time period (48% of ions seen by Geotail), with the bulk of the ions from this source originating closer to Earth, in the region $-10\ R_E > x > -60\ R_E$. The duskside entry of ions for this interval occurs along closed LLBL field lines. Ionospheric particles comprise about 2% of the particles measured by Geotail at this time.

At 1347 UT, Geotail is embedded in a region of closed field lines. Figure 10*b* shows that the source of the ions seen by Geotail is no longer split equally between the dawn and dusk flanks, and the dawnside LLBL is the primary supplier of particles to the Geotail distribution function (88% of ions measured by Geotail). To provide insight into the particle dynamics and access to Geotail during the 1325 UT and 1347 UT time intervals, we plot in Figure 11 the trajectory of a typical particle originating from the duskside LLBL and measured by Geotail at 1347 UT. The upper panel of this figure shows a three-dimensional view of the particle's orbit in GSE coordinates. The black curve in the lower panel shows the particle's kinetic energy (from 0 to 10 keV, scale shown on the left), and the red dots in the lower panel show the particle's parameter of adiabaticity κ (from 0 to 10, scale on the right of the panel) as a function of time [*Büchner and Zelenyi*, 1986]. κ is defined as

$$\kappa = \sqrt{R_c / \rho_L} \tag{2}$$

where R_c is the local magnetic field radius of curvature and ρ_L is the ion Larmor radius. When $\kappa > 1$, particles follow guiding center orbits and are adiabatic. When $\kappa \leq 1$, however, particles no longer conserve their first adiabatic invariant and follow stochastic, or quasi-adiabatic, trajectories. The upper panel of this figure shows that the particle enters

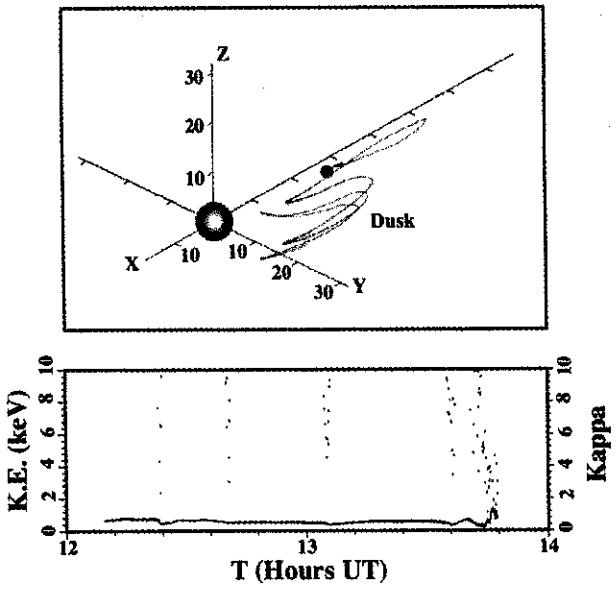

Figure 11. Trajectory of a particle originating in the duskside magnetopause and arriving at Geotail at 1347 UT. The upper panel shows a three-dimensional projection of the particle's orbit, and the lower panel depicts the particle's kinetic energy (black curve, scale on left), and κ (red dots, scale on right).

the magnetosphere at $x \sim -20\ R_E$ on the dusk side of the magnetopause in the region with the largest number of ions entering via the dusk side LLBL. After entering the magnetosphere, the ion is immediately trapped in the near-Earth region. It executes several adiabatic ($\kappa >> 1$) bounces and convects dawnward until it encounters Geotail (shown by a green dot). This orbit is representative of that of the ions entering the magnetosphere on the dusk flank between $-10\ R_E > x > -30\ R_E$ and shows that the bulk of the ions from the duskside source reaches Geotail on trapped orbits. At the same time, the particle's energy does not change significantly and the particle arrives at Geotail with an energy of ~ 2 keV.

Figure 12 shows a particle originating in the dawnside LLBL in a format similar to Figure 11. The three-dimensional rendering of the particle's orbit (upper panel) shows the particle entering the magnetosphere on the dawnside at $x \sim -90\ R_E$ with a kinetic energy of ~ 2 keV. The particle then crosses the magnetotail from dawn to dusk, executes several nonadiabatic ($\kappa \leq 1$) interactions with the current sheet (red dots in lower panel) in which it gains energy, and finally arrives at Geotail (green dot) with an energy of ~ 4 keV. This type of particle accounts for the bulk of the distribution measured in the direction perpendicular to **B** as well as for the warmer perpendicular temperature of the measured distribution compared to that at 1325 UT.

5. SUMMARY AND DISCUSSION

In this paper, we have examined two separate events that are characterized by steady, northward IMF. Using a global MHD calculation driven by IMP-8 and Wind spacecraft solar wind and IMF data we have simulated these events and compared the results with Geotail observations. In the second case (Feb. 9, 1995), we have gone one step further and applied the LSK technique using time-dependent MHD fields and observed distribution functions in order to examine plasma transport and energization.

1. Both examples shown in this paper demonstrate that the magnetosphere responds in a complex, nonlinear way to changes in the IMF and solar wind, and is significantly influenced by the past history of solar wind changes. This can be understood as being a consequence of the interaction between external driving by the solar wind and the IMF and the magnetosphere's internal dynamics.

2. On March 29, 1993, the presence of a changing IMF B_y component causes the magnetotail to become severely twisted and flattened. The longer dimension of the tail cross section follows the changes in the IMF clock angle rapidly, i.e. within a few minutes, such that the semimajor tail axis remains largely aligned with the magnetosheath field direction in the y - z plane. At times, the twisting is so strong that the northern (southern) lobe is displaced to the southern (northern) hemisphere in the distant tail.

3. On February 9, 1995, the IMF B_y component also causes a twisting of the magnetotail current sheet. However, because the IMF B_y is relatively steady during the time interval considered, the effect on the magnetotail is not as drastic as that of March 29, 1993, and the magnetotail cross-section shows very little change as a function of time. Although the IMF shows little variation over several hours, subtle changes in the interior structure of the tail occur owing to its internal dynamics and convection. These changes have a substantial effect on the ion distribution functions, as is evident from the Geotail observations and the LSK calculations.

4. By applying the LSK technique in the February 9, 1995 case, we have been able to examine these changes of the distribution functions in detail. Specifically, we found that

a) At 1325 UT, Geotail was entering a region of closed field lines, allowing ions from both the dawn and dusk side LLBL to gain access to the spacecraft location. Ions from both the duskside and the dawnside sources originated from broad regions in z centered on the equatorial plane which had rotated out of the $z = 0$ plane because IMF $B_y \neq 0$. The ionosphere also made a contribution to the Geotail distribution, supplying ~2% of the measured ions. Ions from the duskside source followed guiding center orbits. However, ions from the dawnside source were characterized by multiple nonadiabatic interactions with the current sheet and accounted for the component of the distribution measured by Geotail in the direction perpendicular to **B**.

b) At 1347 UT, Geotail was embedded in a region of closed field lines. Because the spacecraft entered the outer CPS from the PSBL, it measured more particles from the dawn LLBL so that the dawnside ion source became dominant. It is interesting to note that because of their stochastically trapped orbits, dawn side ions are seen in numbers only when the satellite enters into a region of closed field lines. The ionospheric contribution to the Geotail distribution increased slightly, to ~3% of the measured particles. Once again, dawnside ions moved on principally nonadiabatic trajectories which scattered them in pitch angle and energized them before they arrived at Geotail. The density of particles entering the magnetosphere from the dawnside ion source increased steadily downtail. In contrast, the peak in duskside entry occurred earthward of Geotail. This caused the duskside ions to be trapped in adiabatic trajectories as soon as they entered the magnetosphere and resulted in their arriving at Geotail while moving in the tailward direction.

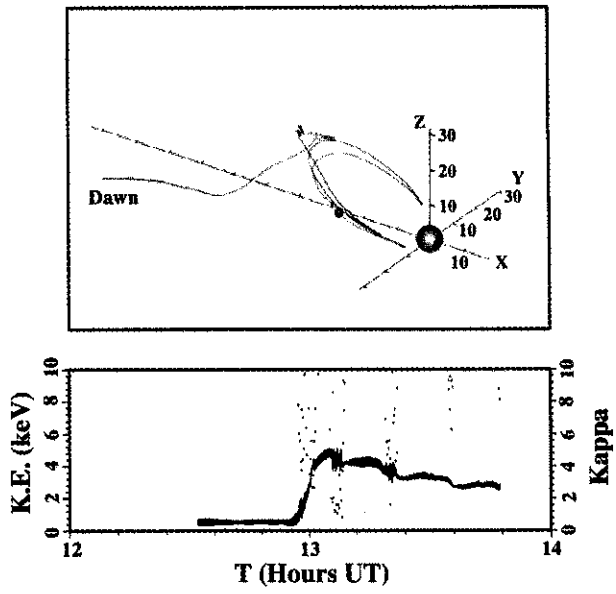

Figure 12. Trajectory of a particle originating on the dawnside and arriving at Geotail at 1347 UT. The format of the figure is similar to that of Fig. 11.

The MHD simulations presented in this paper have shown that the structure of the magnetotail during periods of northward IMF with a significant IMF B_y component is quite different from the picture predicted by simple models and that the overall picture cannot be obtained from a simple superposition of idealized configurations. An analysis of why the magnetotail responds to northward IMF in the manner it does will be provided in a forthcoming paper.

The MHD simulations used in this paper are far from ideal. Using a single point measurement of the solar wind ~200 R_E upstream of Earth does not allow for compensating for structures in the solar wind. For example, structures measured by the Wind spacecraft and used as input for our simulations may never encounter Earth and result in discrepancies between the model and observations. At the same time, the spatial grid used in the simulation is often too coarse to resolve sharp gradients in plasma and magnetic field parameters. Also, we use a simple model for the IMF B_x in our simulations and hold Earth's dipole tilt constant throughout the simulation. Both of these approximations can lead to errors, especially late in the simulation run. Despite these shortcomings we have used MHD simulations simply because they are the best global models available for our purposes.

We have outlined our initial efforts to use the LSK technique along with time-dependent MHD electric and magnetic fields in order to assess the transport and acceleration processes affecting particle behavior in the magnetotail. A natural extension of these efforts would be the application of this technique to more dynamic magnetospheric intervals and to times when there is more than one satellite in the magnetotail. So far, our studies have been limited to periods of northward IMF, but as the magnetosphere is much more active during southward IMF intervals, it represents an interesting challenge to our modeling effort. Similarly, a study using Geotail data together with data from either Polar or Interball would allow us to investigate not only the transport and acceleration of plasma, but would also allow us to gain insight into the subject of common particle sources supplying the magnetospheric regions covered by these spacecraft.

Acknowledgments. We thank J. M. Bosqued, L. A. Frank, W. R. Paterson, R. L. Richard, R. J. Walker, and L. M. Zelenyi for many useful discussions. We also thank L. A. Frank and W. R. Paterson for providing the Geotail distribution functions, K. Ogilvie for providing the Wind plasma data and R. P. Lepping for providing the Wind IMF data. This work was supported by NASA grants NAG5-1100 and NAGW-4553. Computing support was provided by the Cornell Theory Center, the Office of Academic Computing at UCLA, the San Diego Supercomputer Center, and the Maui High Performance Computing Center. UCLA/IGPP publication number 4934.

REFERENCES

Akasofu, S.-I., E. W. Hones, Jr., S. J. Bame, J. R. Asbridge, and A. T. Y. Lui, Magnetotail and boundary layer plasmas at a geocentric distance of ~18 R_E: VELA 5 and 6 observations, *J. Geophys. Res.*, *78*, 7257, 1973.

Ashour-Abdalla, M., J. Berchem, J. Büchner, and L. M. Zelenyi, Shaping of the magnetotail from the mantle: Global and local structuring, *J. Geophys. Res.*, *98*, 5651, 1993.

Ashour-Abdalla, M., L. M. Zelenyi, V. Peroomian, and R. L. Richard, Consequences of magnetotail ion dynamics, *J. Geophys. Res.*, *99*, 14,891, 1994.

Ashour-Abdalla, M., L. M. Zelenyi, V. Peroomian, R. L. Richard, and J. M. Bosqued, The mosaic structure of plasma bulk flows in the Earth's magnetotail, *J. Geophys. Res.*, *100*, 19,191, 1995.

Ashour-Abdalla, M., L. A. Frank, W. R. Paterson, V. Peroomian, and L. M. Zelenyi, Proton velocity distributions in the magnetotail: Theory and observations, *J. Geophys. Res.*, *101*, 2587, 1996.

Ashour-Abdalla, M., M. El Alaoui, V. Peroomian, J. Raeder, R. J. Walker, R. L. Richard, L. M. Zelenyi, L. A. Frank, W. R. Paterson, J. M. Bosqued, R. P. Lepping, K. Ogilvie, S. Kokubun, and T. Yamamoto, Ion sources and acceleration mechanisms inferred from local distribution functions, *Geophys. Res. Lett.*, *24*, 955, 1997.

Balsiger, H., P. Eberhardt, J. Geiss, and D. T. Young, Magnetic storm injection of 0.9 - 16 keV/e solar and terrestrial ions into the high-altitude magnetosphere, *J. Geophys. Res.*, *85*, 1645, 1980.

Berchem, J., J. Raeder, M. Ashour-Abdalla, L. A. Frank, W. R. Paterson, K. L. Ackerson, S. Kokubun, T. Yamamoto, R. P. Lepping, and K. Ogilvie, The distant tail at 200 R_E: Comparisons between Geotail observations and the result of global MHD simulations, *J. Geophys. Res.*, submitted 1997*a*.

Berchem, J., J. Raeder, M. Ashour-Abdalla, L. A. Frank, W. R. Paterson, K. L. Ackerson, S. Kokubun, T. Yamamoto, and R. P. Lepping, Large-scale dynamics of the magnetospheric boundary: Comparisons between global MHD simulation results and ISTP observations, in *Encounter Between Global Observations and Models in the ISTP Era, Geophysical Monograph Series*, J. Horwitz, ed., submitted, 1997*b*.

Büchner, J., and L. M. Zelenyi, Deterministic chaos in the dynamics of charged particles near a magnetic field reversal, *Phys. Lett. A*, *118*, 395, 1986.

Büchner, J., and L. M. Zelenyi, Regular and chaotic charged particle motion in magnetotail-like field reversal, 1, Basic theory of trapped motion, *J. Geophys. Res.*, *94*, 11,821, 1989.

Brecht, S. H., J. G. Lyon, J. A. Fedder, and K. Hain, A simulation study of east-west IMF effects on the magnetosphere, *Geophys. Res. Lett.*, *8*, 397, 1981.

Brecht, S. H., J. G. Lyon, J. A. Fedder, and K. Hain, A time dependent three dimensional simulation of the Earth's magnetosphere: Reconnection events, *J. Geophys. Res.*, *87*, 6098, 1982.

Chappell, C. R., T. E. Moore, and J. H. Waite, Jr., The ionosphere as a fully adequate source of plasma for the Earth's magnetosphere, *J. Geophys. Res.*, *92*, 5896, 1987.

Chen, J., and P. J. Palmadesso, Chaos and nonlinear dynamics of single particle orbits in a magnetotail-like field, *J. Geophys. Res.*, *91*, 1499, 1986.

Cowley, S. W. H., Magnetospheric asymmetries associated with the Y-component of the IMF, *Planet. Space. Sci.*, *29*, 79, 1981.

Eastman, T. E., E. W. Hones, Jr., S. J. Bame, and J. R. Asbridge, The magnetospheric boundary layer: Site of plasma, momentum and energy transfer from the magnetosheath into the magnetosphere, *Geophys. Res. Lett.*, *3*, 685, 1976.

El-Alaoui, M., M. Ashour-Abdalla, J. Reader, J. M. Bosqued, Simulation of ion trajectories in the magnetotail using time-dependent electromagnetic fields, AGU Spring Meeting, Baltimore (EOS, vol. 76, no. 16), 1995.

Fairfield, D. H., Solar wind control of the distant magnetotail: ISEE 3, *J. Geophys. Res.*, 98, 21,625, 1993.

Fairfield, D. H., R. P. Lepping, L. A. Frank, K. L. Ackerson, W. R. Paterson, S. Kokubun, T. Yamamoto, K. Tsuruda, and M. Nakamura, Geotail observations of an unusual magnetotail under very northward IMF conditions, *J. Geomag. Geoelec.*, *48*, 473, 1996.

Fedder, J. A., and J. G. Lyon, The Earth's magnetosphere is 165 R_E long: Self consistent currents, convection, magnetospheric structure and processes for northward interplanetary magnetic field, *J. Geophys. Res.*, *100*, 3623, 1995.

Frank, L. A., K. L. Ackerson, W. R. Paterson, J. A. Lee, M. R. English, and G. L. Pickett, The Comprehensive Plasma Instrumentation (CPI) for the Geotail spacecraft, *J. Geomag. Geoelec.*, *46*, 23, 1994.

Frank, L. A., M. Ashour-Abdalla, J. Berchem, J. Raeder, W. R. Paterson, S. Kokubun, T. Yamamoto, R. P. Lepping, F. V. Coroniti, D. H. Fairfield, and K. L. Ackerson, Observations of plasmas and magnetic field in Earth's distant magnetotail: Comparison with a global MHD model, *J. Geophys. Res.*, *100*, 19,177, 1995.

Geiss, J., H. Balsiger, P. Eberhardt, H. P. Walker, L. Weber, D. T. Young, and H. Rosenbauer, Dynamics of magnetospheric ion composition as observed by the Geos mass spectrometer, *Space Sci. Rev.*, *22*, 537, 1978.

Haerendel, G., G. Paschmann, N. Sckopke, H. Rosenbauer, and P. C. Hedgecock, The frontside boundary layer of the magnetosphere and the problem of reconnection, *J. Geophys. Res.*, *83*, 3195, 1978.

Hardy, D. A., H. K. Hills, and J. W. Freeman, A new plasma regime in the distant geomagnetic tail, *Geophys. Res. Lett.*, *2*, 169, 1975.

Hones, Jr., E. W., J. R. Asbridge, S. J. Bame, M. D. Montgomery, S. Singer, and S.-I. Akasofu, Measurements of magnetotail plasma flow made with Vela 4B, *J. Geophys. Res.*, *77*, 5503, 1972*a*.

Hones, Jr., E. W., S.-I. Akasofu, S. J. Bame, and S. Singer, Outflow of plasma from the magnetotail into the magnetosheath, *J. Geophys. Res.*, *77*, 6688, 1972*b*.

Knight, S., Parallel electric fields, *Planet. Space Sci.*, *21*, 741, 1972.

Kokubun, S., T. Yamamoto, M. H. Acuña, K. Hayashi, K. Shiokawa, and H. Kawano, The Geotail magnetic field experiment, *J. Geomag. Geoelec.*, *46*, 7, 1994.

Leboeuf, J. N., T. Tajima, C. F. Kennel, and J. M. Dawson, Global simulation of the time-dependent magnetosphere, *Geophys. Res. Lett.*, *5*, 609, 1978.

Leboeuf, J. N., T. Tajima, C. F. Kennel, and J. M. Dawson, Global simulations of the three-dimensional magnetosphere, *Geophys. Res. Lett.*, *8*, 257, 1981.

Lennartsson, W., A scenario for solar wind penetration of Earth's magnetic tail based on ion composition data from the ISEE 1 spacecraft, *J. Geophys. Res.*, *97*, 19,221, 1992.

Lennartsson, W., and E. G. Shelley, Survey of 0.1- to 16-keV/e plasma sheet ion composition, *J. Geophys. Res.*, *91*, 3061, 1986.

Lennartsson, W., E. G. Shelley, R. D. Sharp, R. G. Johnson, and H. Balsiger, Some initial ISEE-1 results on the ring current composition and dynamics during the magnetic storm of December 11, 1977, *Geophys. Res. Lett.*, *6*, 483, 1979.

Lennartsson, W., R. D. Sharp, E. G. Shelley, R. G. Johnson, and H. Balsiger, Ion composition and energy distribution during 10 magnetic storms, *J. Geophys. Res.*, *86*, 4628, 1981.

Lepping, R. P., et al., The Wind magnetic field investigation, *Space Sci. Rev.*, *71*, 207, 1995.

Lundin, R., L. R. Lyons, and N. Pissarenko, Observations of the ring current composition at L < 4, *Geophys. Res. Lett.*, *7*, 425, 1980.

Lyon, J, G., S. H. Brecht, J. D. Huba, J. A. Fedder, J. A. Fedder, and P. J. Palmadesso, Computer simulation of a geomagnetic substorm, *Phys. Rev. Lett.*, *46*,1038, 1981.

Lyons, L. R., and T. W. Speiser, Evidence for current sheet acceleration in the geomagnetic tail, *J. Geophys. Res.*, *87*, 2276, 1982.

Lyons, L. R., D. Evans, and R. Lundin, An observed relation between magnetic field aligned electric fields and downward electron energy fluxes in the vicinity of auroral forms, *J. Geophys. Res.*, *84*, 457, 1979.

Martin, R. F., Jr., Chaotic particle dynamics near a two-dimensional neutral point, with application to the Earth's magnetotail, *J. Geophys. Res.*, *91*, 11,985, 1986.

Moen, J., and A. Brekke, The solar flux influence on quiet time conductances in the auroral ionosphere, *Geophys. Res. Lett.*, *20*, 971, 1993.

Ogilvie, K. W., et al., SWE, A comprehensive plasma instrument for the Wind spacecraft, *Space Sci. Rev.*, *71*, 55, 1995.

Ogino, T., and R. J. Walker, A magnetohydrodynamic simulation of the bifurcation of the tail lobes during intervals with a northward interplanetary magnetic field, *Geophys. Res. Lett.*, *11*, 1018, 1984.

Ogino, T., R. J. Walker, M. Ashour-Abdalla, and J. M. Dawson, An MHD simulation of B_y dependent magnetospheric convection and field-aligned currents during northward IMF, *J. Geophys. Res.*, *90*, 10,835, 1985.

Ogino, T., R. J. Walker, and M. Ashour-Abdalla, A global magnetohydrodynamic simulation of the magnetosheath and magnetosphere when interplanetary magnetic field is northward, *IEEE Trans. Plasma Sci.*, *20*, 817, 1992.

Ogino, T., R. J. Walker, and M. Ashour-Abdalla, A global magnetohydrodynamic simulation of the response of the magnetosphere to a northward turning of the interplanetary magnetic field, *J. Geophys. Res.*, *99*, 11,027, 1994.

Peroomian, V., and M. Ashour-Abdalla, Relative contribution of the solar wind and the auroral zone to near-Earth plasmas, in *Cross-Scale Coupling in Space Plasmas*, *Geophysical Monograph Series*, vol. 93, edited by J. Horwitz et al., pp. 213-217, AGU, Washington, D. C., 1995.

Peroomian, V., and M. Ashour-Abdalla, Population of the near-Earth magnetotail from the auroral zone, *J. Geophys. Res.*, *101*, 15,387, 1996.

Peterson, W. K., R. D. Sharp, E. G. Shelley, R. G. Johnson, and H. Balsiger, Energetic ion composition in the plasma sheet, *J. Geophys. Res.*, *86*, 761, 1981.

Pilipp, W. G., and G. Morfill, The formation of the plasma sheet resulting from plasma mantle dynamics, *J. Geophys. Res.*, *83*, 5670, 1978.

Raeder, J., R. J. Walker, and M. Ashour-Abdalla, The structure of the distant geomagnetic tail during long periods of northward IMF, *Geophys. Res. Lett.*, *22*, 349, 1995.

Raeder, J., J. Berchem, and M. Ashour-Abdalla, The importance of small-scale processes in global MHD simulations: Some numerical experiments, in *The Physics of Space Plasmas*, vol. 14, T. Chang and J. R. Jasperse, eds., p. 403, MIT Center for Theoretical Geo/Cosmo Plasma Physics, Cambridge, MA, 1996.

Raeder, J., J. Berchem, M. Ashour-Abdalla, L. A. Frank, W. R. Paterson, K. L. Ackerson, R. P. Lepping, K. Ogilvie, S. Kokubun, T. Yamamoto, and D. H. Fairfield, The distant tail under strong northward IMF conditions: Global MHD results for the Geotail March 29, 1993 observations, *J. Geophys. Res.*, in press, 1997*a*.

Raeder, J., J. Berchem, M. Ashour-Abdalla, L. A. Frank, W. R. Paterson, K. L. Ackerson, J. M. Bosqued, R. P. Lepping, S. Kokubun, T. Yamamoto, S. A. Slavin, Boundary layer formation in the magnetotail: Geotail observations and comparisons with a global MHD model, *Geophys. Res. Lett.*, in press, 1997*b*.

Richard, R. L., R. J. Walker, and M. Ashour-Abdalla, The population of the magnetosphere by solar wind ions when the interplanetary magnetic field is northward, *Geophys. Res. Lett.*, *21*, 2455, 1994.

Robinson, R. M., R. R. Vondrak, K. Miller, T. Dabbs, and D. Hardy, On calculating ionospheric conductances from the flux and energy of precipitating electrons, *J. Geophys. Res.*, *92*, 2565, 1987.

Rosenbauer, H., H. Grünwaldt, M. D. Montgomery, G. Paschmann, and N. Sckopke, Helios 2 plasma observations in the distant polar magnetosphere: The plasma mantle, *J. Geophys. Res.*, *80*, 2723, 1975.

Sharp, R. D., W. Lennartsson, W. K. Peterson, and E. G. Shelley, The origins of the plasma in the distant plasma sheet, *J. Geophys. Res.*, *87*, 10,420, 1982.

Shelley, E. G., R. G. Johnson, and R. D. Sharp, Satellite observations of energetic heavy ions during a geomagnetic storm, *J. Geophys. Res.*, *77*, 6104, 1972.

Shelley, E. G., W. K. Peterson, A. G. Ghielmetti, and J. Geiss, The polar ionosphere as a source of energetic magnetospheric plasma, *Geophys. Res. Lett.*, *9*, 941, 1982.

Sibeck, D. G., G. L., Siscoe, J. A. Slavin, E. J. Smith, and B. T. Tsurutani, and R. P. Lepping, The distant magnetotail's response to a strong interplanetary magnetic field B_y: Twisting, flattening, field line bending, *J. Geophys. Res.*, *90*, 4011, 1985.

Sibeck, D. G., J. A. Slavin, E. J. Smith, and B. T. Tsurutani, Twisting of the geomagnetic tail, in *Solar Wind Magnetosphere Coupling*, edited by Y. Kamide and J. A. Slavin, p. 731, Terra Scientific, Tokyo, 1986.

Song, P. and C. T. Russell, Model of the formation of the low-latitude boundary layer for strongly northward interplanetary magnetic field, *J. Geophys. Res.*, *97*, 1411, 1992.

Speiser, T. W., Particle trajectories in model current sheets, *J. Geophys. Res.*, *70*, 4219, 1965.

Usadi, A., A. Kageyama, K. Watanabe, and T. Sato, A global simulation of the magnetosphere with a long tail: Southward and northward interplanetary magnetic field, *J. Geophys. Res.*, *98*, 7503, 1993.

Walker, R. J., R. L. Richard, and M. Ashour-Abdalla, The entry of solar wind ions into the magnetosphere, in *Physics of the Magnetopause*, *Geophysical Monograph Series*, vol. 90, edited by P. Song et al., pp. 311-319, AGU, Washington, D. C., 1995.

Walker, R. J., R. L. Richard, T. Ogino, and M. Ashour-Abdalla, Solar wind entry into the magnetosphere when the interplanetary magnetic field is southward, in *Physics of Space Plasmas (1995)*, *SPI Conference Proceedings and Reprint Series*, edited by T. Chang, p. 561, MIT, Cambridge, MA, 1996.

Maha Ashour-Abdalla, Joachim Raeder, Mostafa El-Alaoui, Vahé Peroomian, Institute of Geophysics and Planetary Physics, University of California, Los Angeles, CA 90095-1567 (e-mail mabdalla@igpp.ucla.edu).